Washington University School of Medicine
Digital Commons@Becker

Open Access Publications

2018

Caveolin-1 regulates lipid droplet metabolism in endothelial cells via autocrine prostacyclin–stimulated, cAMP-mediated lipolysis

Andrew Kuo
Yale University
Monica Y. Lee
Yale University
Kui Yang
Washington University School of Medicine in St. Louis
Richard W. Gross
Washington University School of Medicine in St. Louis
William C. Sessa
Yale University

Follow this and additional works at: https://digitalcommons.wustl.edu/open_access_pubs
Please let us know how this document benefits you.

Recommended Citation

Kuo, Andrew; Lee, Monica Y.; Yang, Kui; Gross, Richard W.; and Sessa, William C., "Caveolin-1 regulates lipid droplet metabolism in endothelial cells via autocrine prostacyclin–stimulated, cAMP-mediated lipolysis." Journal of Biological Chemistry. 293, 3. 973-983. (2018).
https://digitalcommons.wustl.edu/open_access_pubs/6586

This Open Access Publication is brought to you for free and open access by Digital Commons@Becker. It has been accepted for inclusion in Open Access Publications by an authorized administrator of Digital Commons@Becker. For more information, please contact vanam@wustl.edu.

Caveolin-1 regulates lipid droplet metabolism in endothelial cells via autocrine prostacyclin–stimulated, cAMP-mediated lipolysis

Received for publication, November 15, 2017, and in revised form, November 28, 2017 Published, Papers in Press, December 4, 2017, DOI 10.1074/jbc.RA117.000980

Andrew Kuo[‡§], **Monica Y. Lee**[‡¶], **Kui Yang**[‖**], Richard W. Gross[‖**], and William C. Sessa[‡¶1]

*From the [‡]Vascular Biology and Therapeutics Program and Departments of [¶]Pharmacology and [§]Cell Biology, Yale University School of Medicine, New Haven, Connecticut 06510, the [‖]Department of Medicine and Developmental Biology, Division of Bioorganic Chemistry and Molecular Pharmacology, Washington University School of Medicine, St. Louis, Missouri 63110, and the **Department of Chemistry, Washington University, St. Louis, Missouri 63130*

Edited by George M. Carman

Lipid droplets (LD) are dynamic organelles involved in intracellular lipid metabolism in almost all eukaryotic cells, and LD-associated proteins tightly regulate their dynamics. One LD coat protein is caveolin-1 (Cav-1), an essential component for caveola assembly in highly differentiated cells, including adipocytes, smooth muscle cells, and endothelial cells (EC). However, the role of Cav-1 in LD dynamics is unclear. Here we report that EC lacking Cav-1 exhibit impaired LD formation. The decreased LD formation is due to enhanced lipolysis and not caused by reduced triglyceride synthesis or fatty acid uptake. Mechanistically, the absence of Cav-1 increased cAMP/PKA signaling in EC, as indicated by elevated phosphorylation of hormone-sensitive lipase and increased lipolysis. Unexpectedly, we also observed enhanced autocrine production of prostaglandin I_2 (PGI_2, also called prostacyclin) in Cav-1 KO EC, and this PGI_2 increase appeared to stimulate cAMP/PKA pathways, contributing to the enhanced lipolysis in Cav-1 KO cells. Our results reveal an unanticipated role of Cav-1 in regulating lipolysis in non-adipose tissue, indicating that Cav-1 is required for LD metabolism in EC and that it regulates cAMP-dependent lipolysis in part via the autocrine production of PGI_2.

Caveolae are well-characterized lipid raft microdomains with 60- 100-nm, flask-shaped invagination structure found in highly differentiated cell types, including endothelial cells (EC),[2] adipocytes, smooth muscle cells, and fibroblasts (1). Caveolins, including caveolin-1 (Cav-1), Cav-2, and Cav-3, are the major coat proteins driving caveola biogenesis (2). Among these isoforms, Cav-1 is necessary for caveola assembly in EC and adipocytes because blood vessels and adipose tissue isolated from Cav-1–deficient mice exhibit complete loss of caveolae (3, 4). Caveolae have been implicated in many cellular processes, including cholesterol homeostasis, endocytosis, signal transduction, mechanosensing, and lipid metabolism (2). Physiologically, mice lacking Cav-1 are lean and exhibit lipodystrophy with elevated plasma triglyceride (TG) and cholesterol levels (5). Breeding of Cav-1–deficient mice to atherosclerotic mice markedly reduces the extent of atherosclerosis and reduces the infiltration of LDLs into the artery wall in the face of elevated plasma lipids (6, 7). Importantly, reintroducing Cav-1 only into EC reverses these phenotypes, showing the significance of Cav-1 in EC during atherogenesis (7). These results suggest a potential role of Cav-1 in regulating endothelial lipid metabolism, although it has not been investigated in significant detail.

Lipid droplets (LD) are phospholipid monolayer spheres that function as intracellular sites for neutral lipid storage. LD are prominently expressed in energy-storing cell types such as adipocytes and hepatocytes; however, almost all eukaryotic cells are capable of forming and metabolizing LD (8). LD dynamics are regulated by the recruitment of key molecules promoting fatty acid storage and metabolism. For instance, diglyceride acyltransferase 2 (DGAT2), the rate-limiting enzyme catalyzing TG synthesis, translocates to the surface of LD and promotes TG storage into cytosolic LD (9). CTP:phosphocholine cytidyltransferase, a key enzyme of phospholipid synthesis, is also found on the surface of LD and can regulate LD size (10). Notably, Cav-1 has been localized to LD in several cell types (11–13), and in adipocytes, Cav-1 can regulate LD homeostasis in a perilipin (PLN)-dependent (14) and a lipid-induced mechanosensitive manner (15). However, it is still not fully understood how Cav-1 regulates LD dynamics, particularly in non-adipose tissue such as EC.

Our recent work demonstrated that EC exhibit the machinery to form LD and that these LD are coated with Cav-1 (16). In this study, we report that the loss of Cav-1 in EC reduces the number and TG content of LD and that this is due to enhanced ATGL-dependent lipolysis but not reduced TG synthesis or FA

This work was supported by National Institutes of Health Grants R01 HL64793, R01 HL61371, and P01 HL1070295; a MERIT award from the American Heart Association and the Leducq Fondation (MIRVAD Network) (to W. C. S.), and National Institutes of Health Grant R01 HL118639 (to R. W. G.). The authors declare that they have no conflicts of interest with the contents of this article. The content is solely the responsibility of the authors and does not necessarily represent the official views of the National Institutes of Health.

[1] To whom correspondence should be addressed: Vascular Biology and Therapeutics Program, Yale University School of Medicine, 10 Amistad St., New Haven, CT 06520. Tel.: 203-737-2291; Fax: 203-737-2290; E-mail: william.sessa@yale.edu.

[2] The abbreviations used are: EC, endothelial cell(s); TG, triglyceride(s); LD, lipid droplet(s); PLN, perilipin; ATGL, adipocyte triglyceride lipase; PGI_2, prostaglandin I_2; OA, oleic acid; DGAT, diglyceride acyltransferase; DAG, diacylglycerol; AC, adenylate cyclase; FSK, forskolin; HSL, hormone-sensitive lipase; Indo, indomethacin; CREB, cAMP-response element-binding protein; AA, arachidonic acid; ANOVA, analysis of variance; FA, fatty acid(s); eNOS, endothelial NOS.

Downloaded from http://www.jbc.org/ at Washington University on March 3, 2018

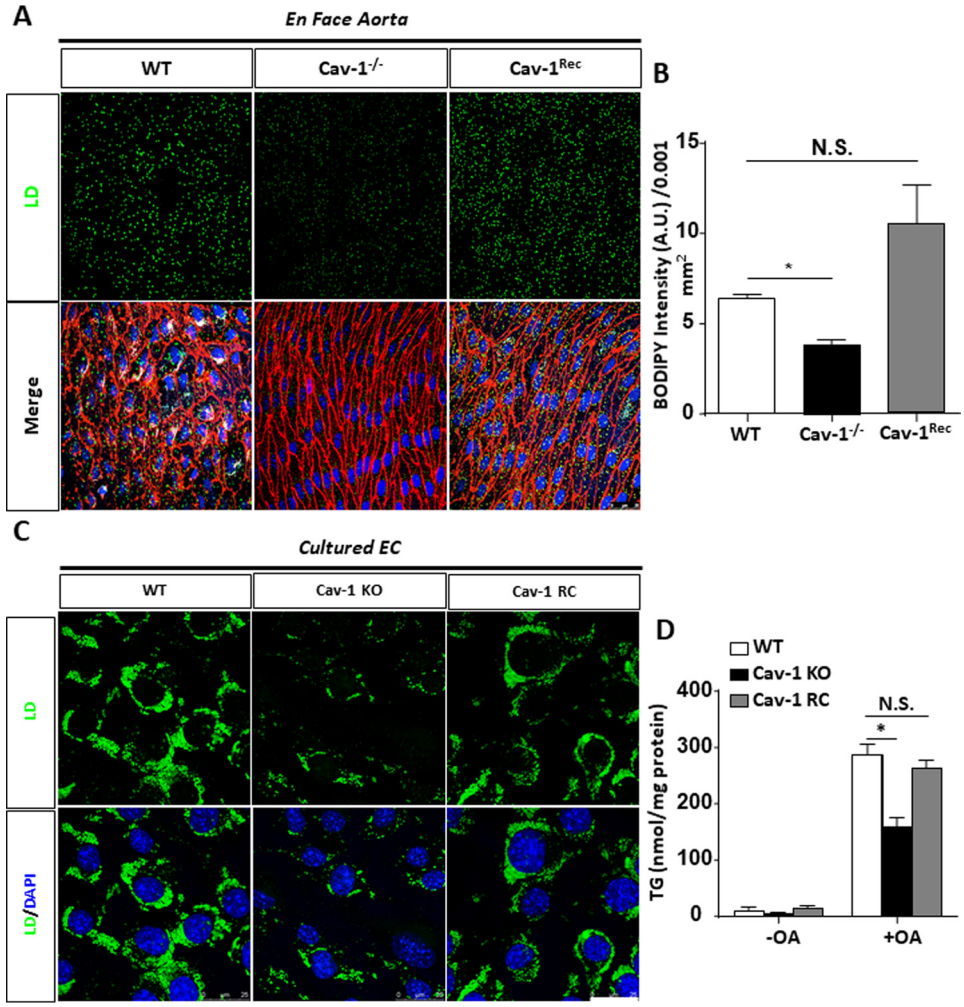

Figure 1. Cav-1 is necessary for LD metabolism and TG content in EC. *A*, thoracic aortae from WT, Cav-1$^{-/-}$, and Cav-1^{Rec} mice were prepared *en face* and immunostained with PECAM-1 (*red*). LD were detected with BODIPY 493/503 (*green*) and nuclei by DAPI (*blue*). Representative z-stack confocal images show that LD formation was reduced in Cav-1$^{-/-}$ aortae and recovered in Cav-1^{Rec} aortae. *B*, quantification of BODIPY intensities from images in *A*. *A.U.*, arbitrary units. *C*, EC isolated from WT, Cav-1 KO, and Cav-1 RC mice were incubated with OA (1 mM) overnight. LD were counterstained in *green* (BODIPY 493/503) and nuclei in *blue* (DAPI). Representative images show that LD formation was impaired in Cav-1 KO EC compared with WT and Cav-1 RC. *D*, quantification of TG content from the samples in *C*. Scale bar in *en face* aortic samples = 50 μm. Scale bar in cultured EC samples = 25 μm. Data are expressed as mean ± S.E. (n = 3 to 4) for *B* and *D*. Statistical analysis was determined by unpaired *t* test. *, $p < 0.05$; *N.S.*, non-significant.

uptake. Mechanistically, the loss of Cav-1 increases cAMP/PKA signaling in EC, potentially because of the autocrine production of PGI_2. Consequently, our results document an unanticipated role of Cav-1 in regulating lipolysis in EC.

Results

Endothelial Cav-1 is an LD-associated protein and necessary for LD formation

Cav-1 is present in isolated LD from endothelial cells (16). To study the functional role of endothelial Cav-1 in LD formation, aortae were isolated from mice with the genotypes WT (C57Bl6), Cav-1$^{-/-}$ (congenic C57Bl6 background), and Cav-1$^{-/-}$ reconstituted with endothelial Cav-1 transgenically (Cav-1^{Rec}, congenic C57Bl6 background) (7) and incubated with oleic acid (OA) for *en face* analysis of LD formation as described previously (16). Cav-1$^{-/-}$ aortae showed reduced LD accumulation in EC, and this defect was rescued in Cav-1^{Rec} aortae (Fig. 1*A*, quantified in Fig. 1*B*). These experiments were complemented in murine lung EC isolated from WT, Cav-1$^{-/-}$ (Cav-1 KO), and Cav-1^{Rec} (Cav-1 RC) mice (17, 18), where loss of Cav-1 impaired LD formation (Fig. 1*C*; triglycerides quantified in Fig. 1*D*). These results suggest that Cav-1 is critical for LD formation in EC.

Cav-1 does not affect fatty acid uptake or TG synthesis in EC

A previous study in mouse embryonic fibroblasts demonstrated that Cav-1 regulates FA uptake via the levels of the fatty acid transporter CD36 (19). Therefore, we tested whether Cav-1 regulates LD formation by mediating FA uptake and CD36 levels in EC. The loss of Cav-1 had no effect on the time-dependent uptake of [^{14}C]oleate into EC (Fig. 2*A*). Immunoblotting of CD36 and FATP4, a major long-chain FA transporter in EC, showed comparable abundance among the genotypes (Fig. 2*B*), implying that endothelial Cav-1 regulates LD formation without affecting the FA uptake or expression of these FA transporters.

Next we tested whether Cav-1 influenced TG synthesis, thereby regulating LD formation. DGAT activity was measured

Downloaded from http://www.jbc.org/ at Washington University on March 3, 2018

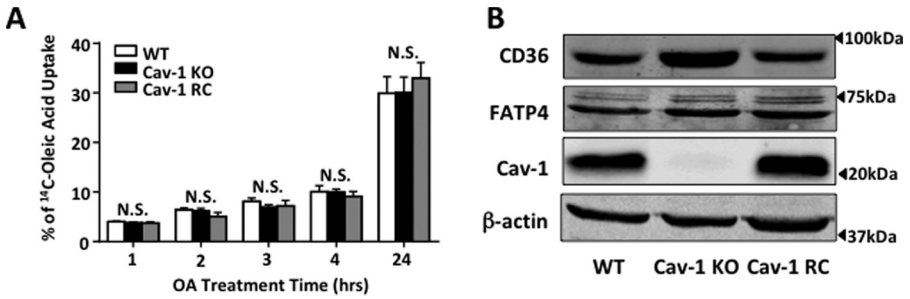

Figure 2. FA uptake is not affected in Cav-1–deficient EC. *A*, FA uptake analysis using radiolabeled [^{14}C]OA suggests that there was no difference of FA uptake between three genotypes of MLEC up to 24 h. *B*, Western blot analysis of fatty acid translocase CD36 and fatty acid transporter protein FATP4 in EC from three genotypes indicates similar abundance. Data are expressed as mean ± S.E. ($n = 3$ individual experiments). Statistical analysis was determined by two-way ANOVA. *N.S.*, not significant.

using [^{14}C]oleoyl-CoA and diacylglycerol (DAG) as co-substrates for TG synthesis, and the formation of radioactive TG was assessed by TLC. As seen in Fig. 3, *A* and *B*, the formation of TG was similar among the three cell types, as was the DAG dependence of the TG formation (Fig. 3, *C* and *D*). Additionally, analysis of the content of fatty acyl species in TG by mass spectrometry showed that Cav-1 KO EC had decreased content of all fatty acyl species measured in TG before and after OA treatment (Fig. 4*A*). Although Cav-1 KO EC exhibited slight differences in the percentage of C16.0 and C20.4 FA of TG when cultured with basal medium, the fatty acyl composition of TG was similar to WT and Cav-1 RC EC after OA treatment (Fig. 4*B*), indicating that the nature of the fatty acids in TG is not affected in the absence of Cav-1.

Lipolysis is augmented in the absence of Cav-1

Next we assessed whether the loss of Cav-1 influenced TG lipolysis. EC were loaded with OA, followed by removal of the fatty acid, and the time-dependent release of fatty acid and glycerol into the medium was examined. Indeed, Cav-1 KO EC released more FA and glycerol over time than WT EC, and the effect in Cav-1 KO EC was normalized in Cav-1 RC cells (Fig. 5, *A* and *B*). The increased metabolism of TG was supported by direct measurement of lipase activity, where Cav-1 KO EC had higher activity that was blunted by the adipocyte triglyceride lipase (ATGL) inhibitor Atglistatin (Fig. 5*C*). Finally, inhibiting ATGL during OA treatment resulted in normalized TG accumulation in all three types of EC (Fig. 5*D*) as well as the presence of LD via imaging (Fig. 5*E*), suggesting that loss of Cav-1 in EC enhanced lipolysis and consequently led to reduced LD formation.

Cav-1 negatively regulates lipolysis in a cAMP-PKA–dependent mechanism

In adipocytes, lipolysis can be induced by agonists that couple via the G protein α subunit G_s to adenylate cyclase (AC) activating the cAMP-mediated PKA pathway. To examine whether Cav-1 influenced the cAMP-PKA pathway in EC, intracellular cAMP levels were measured during OA loading. As seen in Fig. 6*A*, Cav-1 KO cells exhibited higher basal and OA-loaded cAMP levels compared with WT or Cav-1 RC EC. Examination of PKA-mediated substrate phosphorylation with a PKA substrate motif (RR*X*S*/T*) antibody indicated elevated levels of PKA phosphorylation of multiple proteins upon OA incubation in Cav-1 KO EC (Fig. 6*B*). Next, we assessed forskolin (FSK) activation of AC and the phosphorylation of PKA substrates in EC. FSK induced the phosphorylation of CREB-1 at Ser-133 and eNOS at Ser-635 to a greater extent in Cav-1 KO EC (Fig. 6*C*; quantified in Fig. 6, *D* and *E*) compared with WT and Cav-1 RC cells, implying that endogenous Cav-1 negatively regulated AC-PKA signaling in EC.

To determine whether the elevated cAMP/PKA signaling pathway regulated lipolysis in EC, PKA-mediated phosphorylation of hormone-sensitive lipase (HSL on Ser-563) (20, 21), a known regulator of lipolytic flux, was examined. EC were loaded with OA overnight, followed by stimulation with FSK for 0–30 min. OA loading increased basal HSL and CREB-1 phosphorylation, and treatment with FSK increased phosphorylation further in Cav-1 KO EC compared with WT and Cav-1 RC EC (Fig. 7*A*; quantified in Fig. 7, *B* and *C*). The increase in PKA activity was not due to changes in levels of PKA subunits, including catalytic PKACα and regulatory RI α/β subunits (Fig. 7*A*). Next, FSK-mediated lipolysis (measured as glycerol release) in OA-loaded cells was measured. The loss of Cav-1 KO EC increased FSK-stimulated glycerol release (Fig. 7*D*), an effect attenuated by inhibition of PKA with H-89 (Fig. 7*E*). Similarly, H-89 treatment during OA treatment also increased TG accumulation in Cav-1 KO EC to a greater extent than in WT and Cav-1 RC (Fig. 7, *F* and *G*). Taken together, these results suggest that loss of Cav-1 in EC augments PKA activity, resulting in enhanced lipolysis and impaired LD formation.

Basal and OA-stimulated increases in PGI_2 contribute to lipolysis in EC

The enhanced basal levels of cAMP, PKA-mediated phosphorylation, and lipolysis in Cav-1 KO EC suggested that perhaps Cav-1 KO cells generated a mediator that promoted autocrine activation of the cAMP-PKA pathway. In EC, the major arachidonic acid metabolite generated via COX) is prostaglandin I_2 (PGI_2, also called prostacyclin). PGI_2 binds to its cognate G protein–coupled receptor (IP), which couples through G_s to AC and PKA activation (22). Indeed, Cav-1 KO EC produced more PGI_2 (as assessed by the stable metabolite 6-keto PGF 1α) under basal and OA-stimulated conditions, which was abolished by blockade of COX using indomethacin (Indo) (Fig. 8*A*). Treatment with Indo or the IP receptor antagonist CAY10441 increased absolute and relative TG levels during OA loading in Cav-1 KO cells (Fig. 8, *B* and *C*). Interestingly, treatment with

Downloaded from http://www.jbc.org/ at Washington University on March 3, 2018

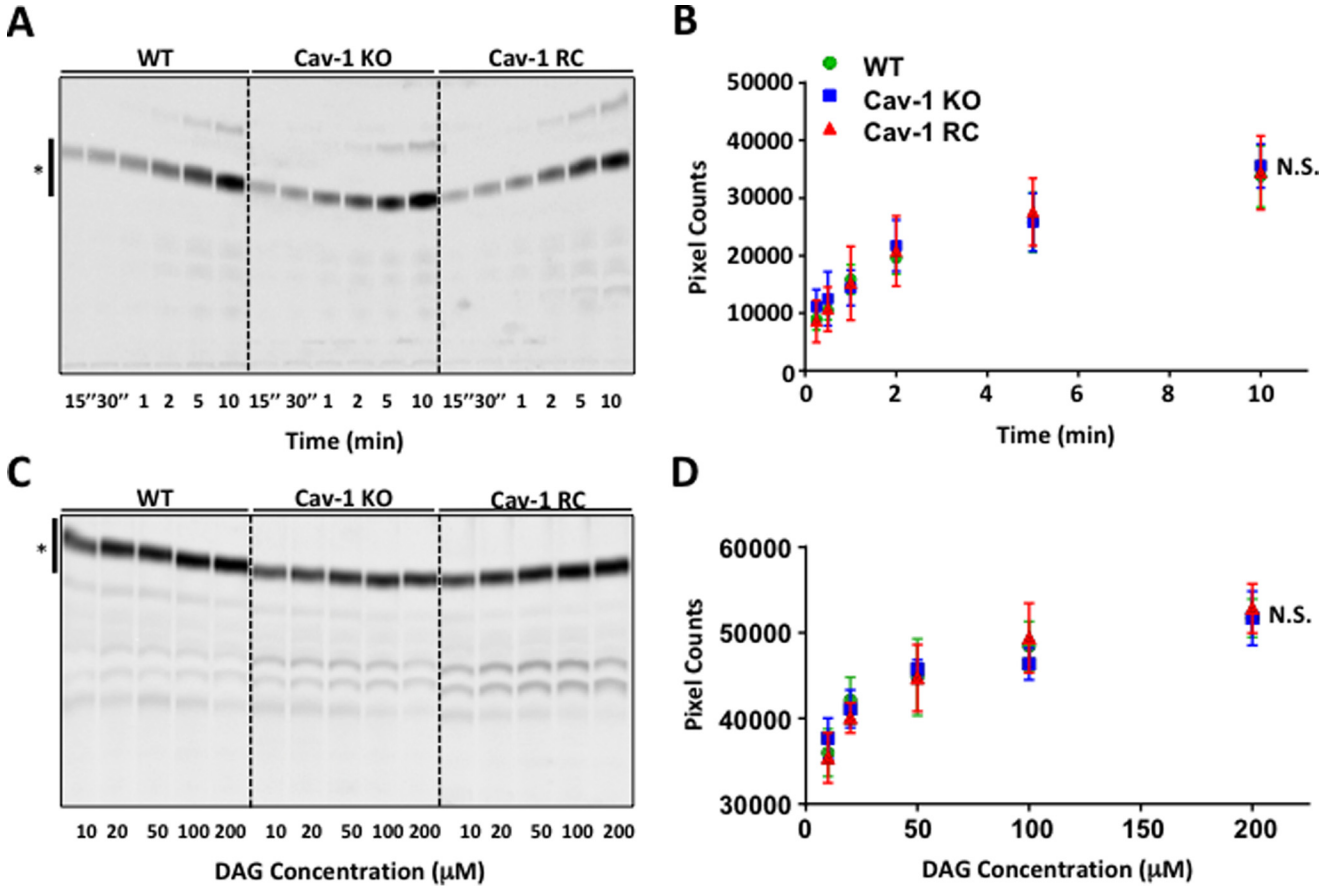

Figure 3. DGAT activity is not affected in the absence of Cav-1. *A*, DGAT activity of whole-cell lysates from three types of EC was measured using exogenous DAG (200 μM) and [^{14}C]oleoyl CoA as co-substrates. Representative thin-layer chromatography images show no difference in TG formation among three types of EC. The band marked by an *asterisk* indicates that TG formed from 15 s to 10 min. *B*, densitometry in designated areas was determined by ImageJ software. *C*, DAG dependence of DGAT activity in three types of MLEC was measured 5 min after addition of [^{14}C]oleoyl CoA and the indicated concentration of DAG. Representative TLC images show no difference in TG formation among three types of MLEC. The band marked by an *asterisk* indicates TG synthesis from 10 to 200 μM. *D*, densitometry in the designated areas was determined by ImageJ software. Data are expressed as mean ± S.E. ($n = 4$ experiments). Statistical analysis was determined by two-way ANOVA in *B* and *D*. *N.S.*, non-significant.

CAY10441 reduced elevated FA and glycerol release in Cav-1 KO cells (Fig. 8, *D* and *E*). These data suggest that the autocrine production of PGI_2 acts as a stimulus for the activation of the cAMP/PKA pathways, contributing to the enhanced lipolysis in Cav-1 KO cells.

Discussion

The central finding of this study shows that Cav-1, an important structural component essential for the assembly of caveola organelles, is necessary for LD metabolism in EC and that it regulates cAMP-dependent lipolysis in part via the autocrine production of PGI_2. Previous studies in adipocytes have highlighted the role of Cav-1 in lipid metabolism in regulating aspects of fatty acid uptake and LD size (23); however, the role of Cav-1 in regulating LD in EC has not been studied until now. Recent work has shown that Cav-1 is enriched in purified LD from EC, and LD in EC serve as reservoirs for neutralizing toxic lipids and can readily metabolize their TG to release FA for energy or utilization by other cells (16).

Global Cav-1 KO mice are lean with hypertriglyceridemia (5), and their adipocytes are smaller with less LD accumulation (13, 14). Mechanistically, the reduction in LD size was linked to defective FA uptake through the fatty acid–binding protein CD36 in adipocytes and in fibroblasts (13, 19, 24). Moreover, the loss of Cav-1 reduces CD36 levels in whole-protein lysates prepared from Cav-1 KO aortic tissue (6). In contrast to previous work, the loss of Cav-1 in intact vessels and in isolated EC reduces LD formation in EC by virtue of enhancing LD degradation but not the uptake of FA or synthesis of TG, effects rescued by genetic reconstitution of Cav-1 back into EC. In isolated EC, the time-dependent uptake of labeled [^{14}C]OA as well as CD36 and FATP4 protein levels are not affected by the loss of Cav-1. In addition to TG synthesis data, MS data confirm that that the composition of fatty acyl groups within TG is not affected by the loss of Cav-1. However, we did not test whether phospholipid composition is altered in LD isolated from Cav-1 KO EC, as demonstrated previously in Cav-1–deficient adipocytes (25).

Surprisingly, the metabolism of TG quantified by the release of glycerol and FA is enhanced in Cav-1 KO EC, explaining why Cav-1 KO EC have fewer TG-rich LD. Enhanced lipolysis during OA loading in Cav-1KO EC is normalized by chemical inhibition of ATGL, implying that Cav-1 modulates LD formation by regulating lipolysis. The loss of Cav-1 in EC enhances OA- and FSK-stimulated cAMP levels and PKA substrate phosphorylation (including HSL, CREB, and eNOS), and enhanced lipol-

Downloaded from http://www.jbc.org/ at Washington University on March 3, 2018

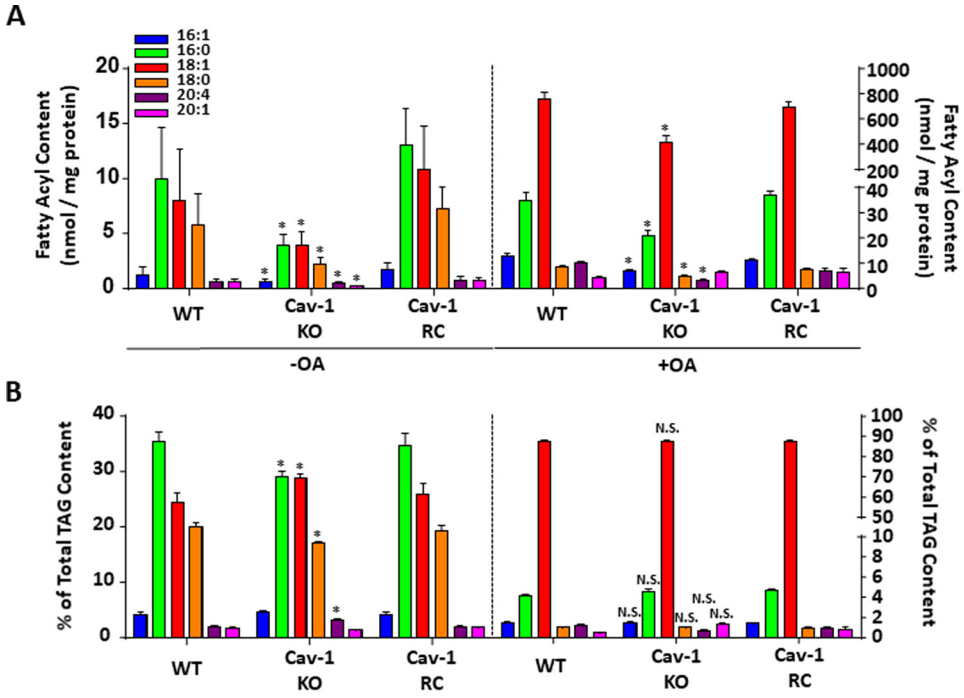

Figure 4. TG composition in LD is not altered in EC lacking Cav-1. *A*, fatty acyl species within TG from three types of EC without or with OA treatment (1 mM) were quantified by mass spectrometry. The content of fatty acyl species in Cav-1 KO EC shows a reduced amount of fatty acyl species in general before OA loading (−*OA*). After OA treatment, 18.1 FA became the predominant species in all three types of EC, with a reduced amount in Cav-1 KO EC (+*OA*). *B*, the composition of fatty acyl species in TG among three types indicates a slightly reduced percentage of C16.0 and C18.0 and increased percentage of C18.1 and C20.4 in Cav-1 KO MLEC (−*OA*). After OA treatment, the composition of fatty acyl species in three types of MLEC is similar (+*OA*). Data are expressed as mean ± S.E. ($n = 4$). Statistical analysis was determined by two-way ANOVA.

ysis in Cav-1 KO EC is normalized by inhibition of PKA. These findings in EC are in contrast to prior work showing blunted lipolytic responses in Cav-1 KO adipocytes in response to β3 receptor agonists or FSK. Impaired lipolysis in Cav-1-deficient adipocytes was mediated via defective cAMP/PKA-dependent phosphorylation of PLN1 and HSL (14, 26). Because PLN1 is expressed exclusively in adipocytes and is not found in EC (16), a different mechanism must exist in non-adipose cell type such as EC. Although PLN2 (formally named ADRP) is thought to be functionally equivalent to PLN1 in non-adipocytes, the molecular regulation of ADRP in lipolysis remains unclear, including its regulation by PKA signaling and HSL. Nevertheless, our results clearly demonstrate that HSL protein levels are elevated in Cav-1–deficient EC and that its phosphorylation is enhanced by FSK treatment, demonstrating a unique mechanism of Cav-1 regulation of lipolysis in endothelium *versus* adipocytes.

The increase in basal and OA-stimulated cAMP in Cav-1 KO EC prompted the search for factors that are produced by EC and regulate cAMP signaling. We show that OA treatment enhances 6-keto PGF1α release in EC, an unexpected link between FA metabolism and prostacyclin production. This idea is supported by a recent study showing that storage-operated calcium entry regulates lipolysis via cAMP up-regulation (28); thus it is possible that enhanced PGI_2 production occurs as a result of enhanced extracellular calcium entry and adenylyl cyclase activation during OA loading. Furthermore, our results show marked release of 6-keto PGF1α in Cav-1 KO EC, suggesting that Cav-1 can regulate aspects of arachidonic acid (AA) release or COX metabolism. A relationship between Cav-1 and AA metabolism in EC has been suggested because COX-2 expression and PG metabolites are elevated in lungs from Cav-1–deficient mice because of loss of COX-2 degradation (29). Moreover, a recent MS study indicated that silencing Cav-1 in EC increases intracellular FFA, including AA metabolites (30). Importantly, in our experiments, both indomethacin and the IP receptor antagonist rescue LD formation in Cav-1 KO EC, implying that autocrine production of PGI_2 can contribute to regulation of PKA and that lipolysis in EC and Cav-1 functions as an endogenous break on the system.

In conclusion, we describe a novel pathway for Cav-1–mediated cAMP activation in EC and a connection between prostacyclin production and lipolysis. Perhaps elevated prostacyclin and the attendant changes in EC lipolysis contribute to the well-established findings that Cav-1 KO mice are protected from atherosclerosis in the face of elevated lipids (6, 7). Additional experiments examining LD metabolism in EC-specific conditional Cav-1–deficient mice will improve our understanding of how Cav-1 regulates LD homeostasis during atherogenesis.

Experimental procedures

Reagents and antibodies

Oleic acid, Atglistatin, forskolin, CAY10499, CAY10441, H-89, isobutylmethylxanthine, and indomethacin were purchased from Cayman Chemical. BODIPY 493/503 was obtained from Life Technologies. The antibodies used in this study were from the following resources, with the indicated dilution for Western blotting: anti-Cav-1 (BD Biosciences,

Downloaded from http://www.jbc.org/ at Washington University on March 3, 2018

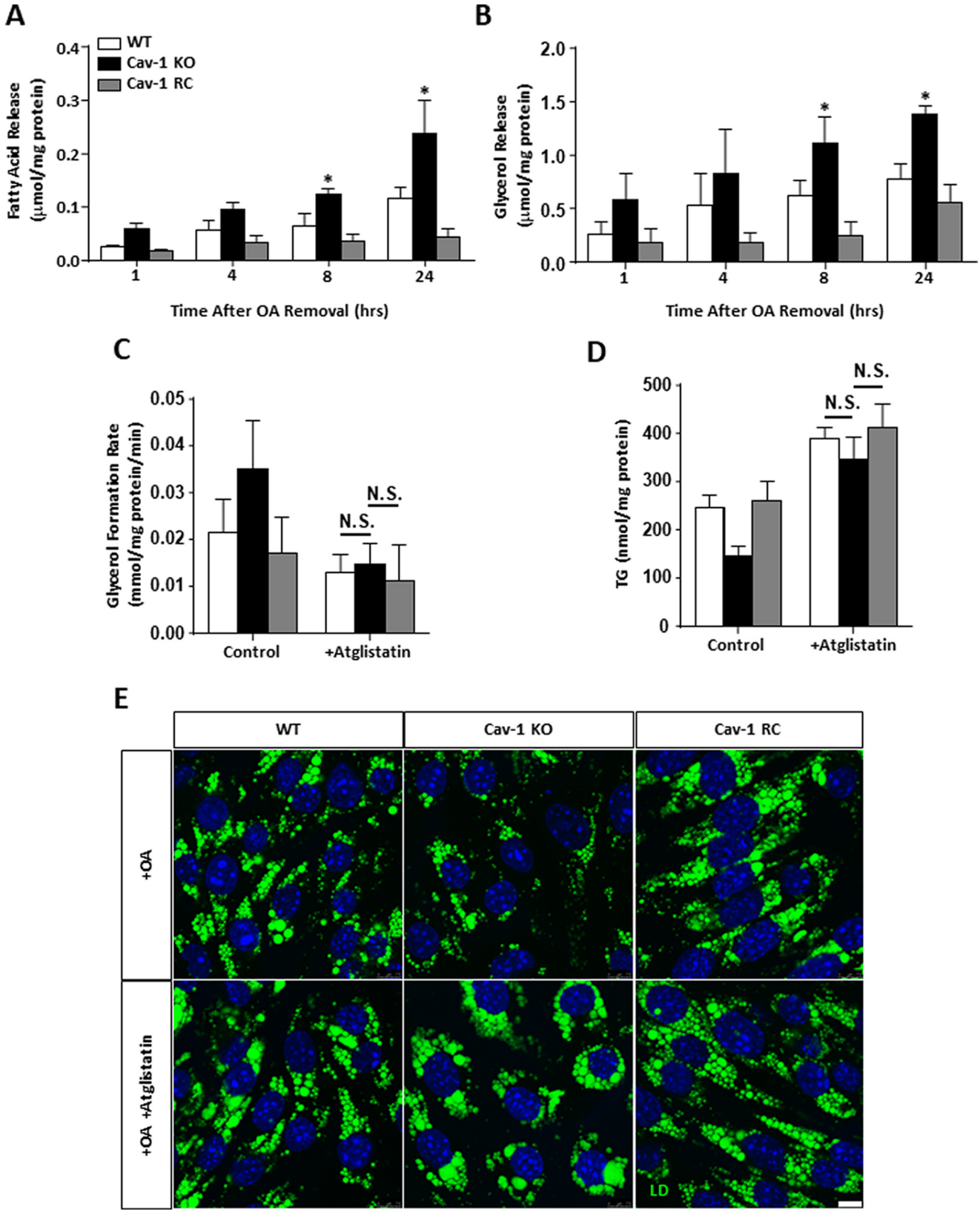

Figure 5. Lipolysis is augmented in Cav-1 KO EC. *A* and *B*, EC were pretreated with OA (1 mM) overnight, and FFA and glycerol release was measured. Cav-1 KO EC show increased release of FFA (*A*) and glycerol (*B*) after 8 h. *C*, general lipase activity from three types of LD-enriched EC was determined by glycerol formation rate. Lysates from Cav-1 KO EC showed increased lipase activity (*Control*), where Atglistatin abolished this induction. *D*, TG content after OA loading of EC in the absence (*Control*) or presence of Atglistatin. *E*, LD were counterstained in *green* (BODIPY 493/503) and nuclei in *blue* (DAPI). Representative images show that inhibition of ATGL by Atglistatin rescued LD formation in Cav-1 KO MLEC to comparable levels of WT and Cav-1 RC ($n = 2$). *Scale bar* = 7.5 μm. Data are expressed as mean ± S.E. ($n = 4\sim5$). Statistical analysis in *A* and *B* was performed by two-way ANOVA. Statistical analysis in *C* and *D* was determined by unpaired *t* test. *N.S.*, non-significant. *, $p < 0.05$ relative to WT and Cav-1 RC.

Downloaded from http://www.jbc.org/ at Washington University on March 3, 2018

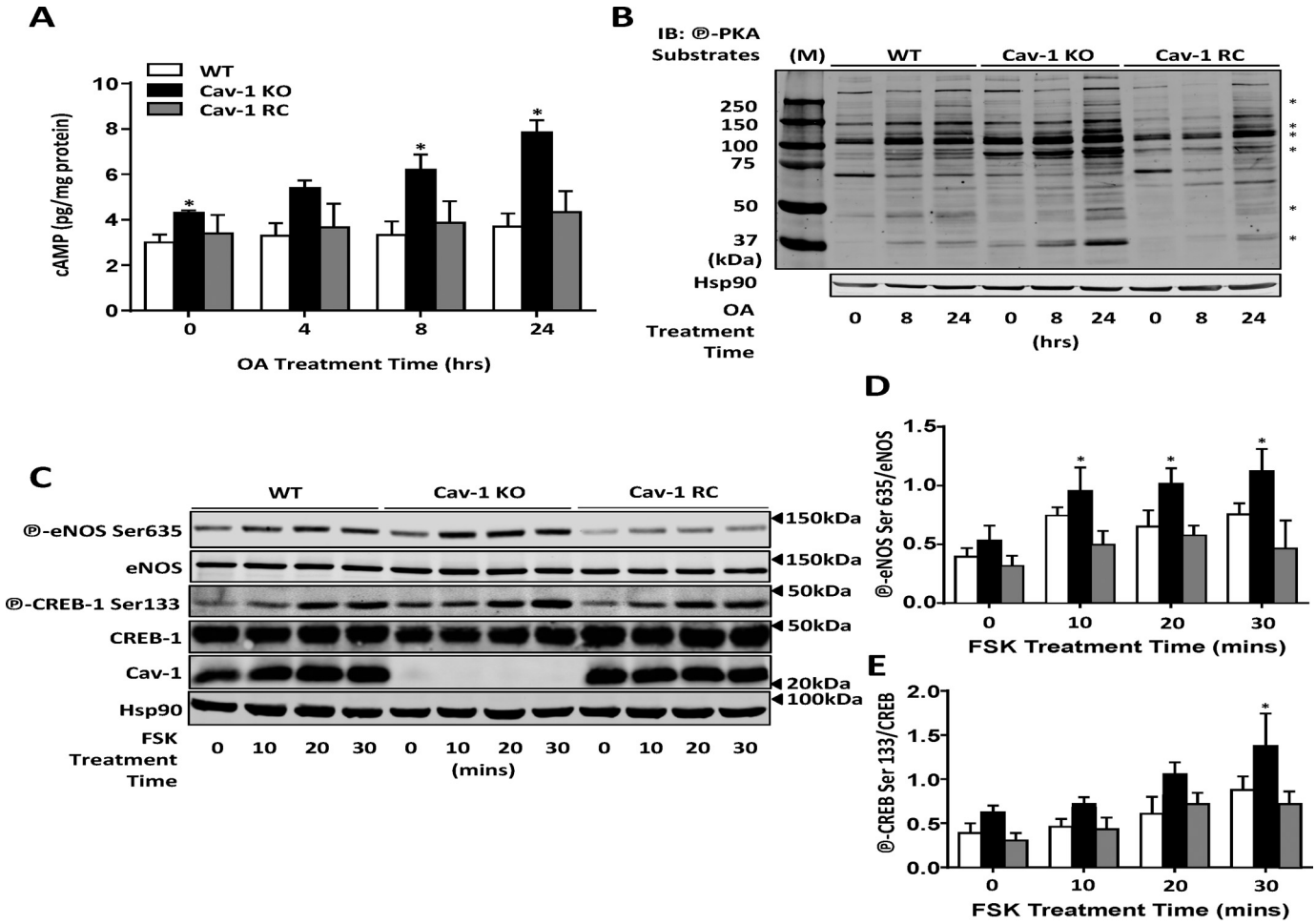

Figure 6. cAMP/PKA signaling is enhanced in Cav-1 KO EC. *A*, intracellular cAMP accumulation was measured over time after OA treatment. Cav-1 KO EC show increased cAMP levels at baseline and after 8-h treatment. *B*, phosphorylation of PKA substrates (*asterisk* bands) in response to OA treatment (1 mM) was detected with a PKA substrate motif (RR*X*S*/T*) antibody. Cav-1 KO EC show stronger enhancement of several bands. *C*, activation of adenylate cyclase with FSK (10 μM) increased phosphorylation of the PKA substrates eNOS at Ser-635 and CREB-1 at Ser-133 in Cav-1 KO MLEC, as quantified in *D* and *E*. Data are expressed as mean ± S.E. ($n = 3$). Western blot images are representative of three independent experiments. Statistical analysis was determined by two-way ANOVA. *, $p < 0.05$ relative to WT and Cav-1 RC.

610060, 1:5000), anti-β-actin (Sigma, A5441, 1:5000), anti-ATGL (Cell Signaling Technology, 2138, 1:1000), anti-CGI58 (Santa Cruz Biotechnology, sc-100468, 1:250), anti-Hsp90 (BD Biosciences, 610419, 1:2000), anti-FATP4 (BioVision Inc., 3268-100, 1:1000), anti-CD36 (Santa Cruz Biotechnology, sc-9154. 1:100 for Western blotting), anti-phospho-PKA substrate (Cell Signaling Technology, 9624, 1:1000), anti-phospho-HSL Ser-563 (Cell Signaling Technology, 4139, 1:500), anti-HSL (Cell Signaling Technology, 4107, 1: 500), anti-phospho-CREB Ser-133 (Santa Cruz Biotechnology, sc-7978, 1:1000), anti-CREB (Santa Cruz Biotechnology, sc-186, 1:250), anti PKA RI α/β (Cell Signaling Technology, 3927, 1:1000), PKACα (Cell Signaling Technology, 4782. 1:1000), anti-phospho-eNOS Ser-635 (EMD Millipore, 07-562, 1:1000), and anti-eNOS (BD Biosciences, 610297, 1:2000).

Animals

Cav-1$^{-/-}$ and Cav-1$^{-/-}$ mice carrying the canine Cav-1 transgene under the preproendothelin-1 promoter (Cav-1^{Rec}) were generated as reported previously (17, 18). All mouse strains were congenic on a C57Bl6 background and maintained on pelleted rodent chow with free access to water. Mice were maintained in a specific pathogen–free animal facility with a steady-temperature room (25 °C) under a fixed 12-h light/dark cycle. All procedures were approved by the Institutional Animal Care and Use Committee of Yale University.

Cell lines

Mouse lung endothelial cells (EC) from C57BL/6 (WT), Cav-1$^{-/-}$ (Cav-1 KO), and Cav-1^{Rec} (Cav-1 RC) mice were isolated and immortalized with middle T antigen as described previously (17, 18). EC lines were cultured in EGM-2 medium (Lonza) containing 20% FBS and supplemented with the SingleQuots^{TM} Kit (Lonza), penicillin/streptomycin, and 2 mM L-glutamine.

Western blot analysis

Cells were washed with PBS three times and lysed with lysis buffer (50 mM Tris-HCl (pH 7.4), 0.1% SDS, 0.1% sodium deoxycholate, 0.1 mM EDTA, 0.1 mM EGTA, 1% Nonidet P-40, 1.5 mg/ml protease inhibitor tablet (Roche), 0.25 mg/ml Pefabloc (Roche), and 50 mM sodium fluoride.) Lysates were incu-

Downloaded from http://www.jbc.org/ at Washington University on March 3, 2018

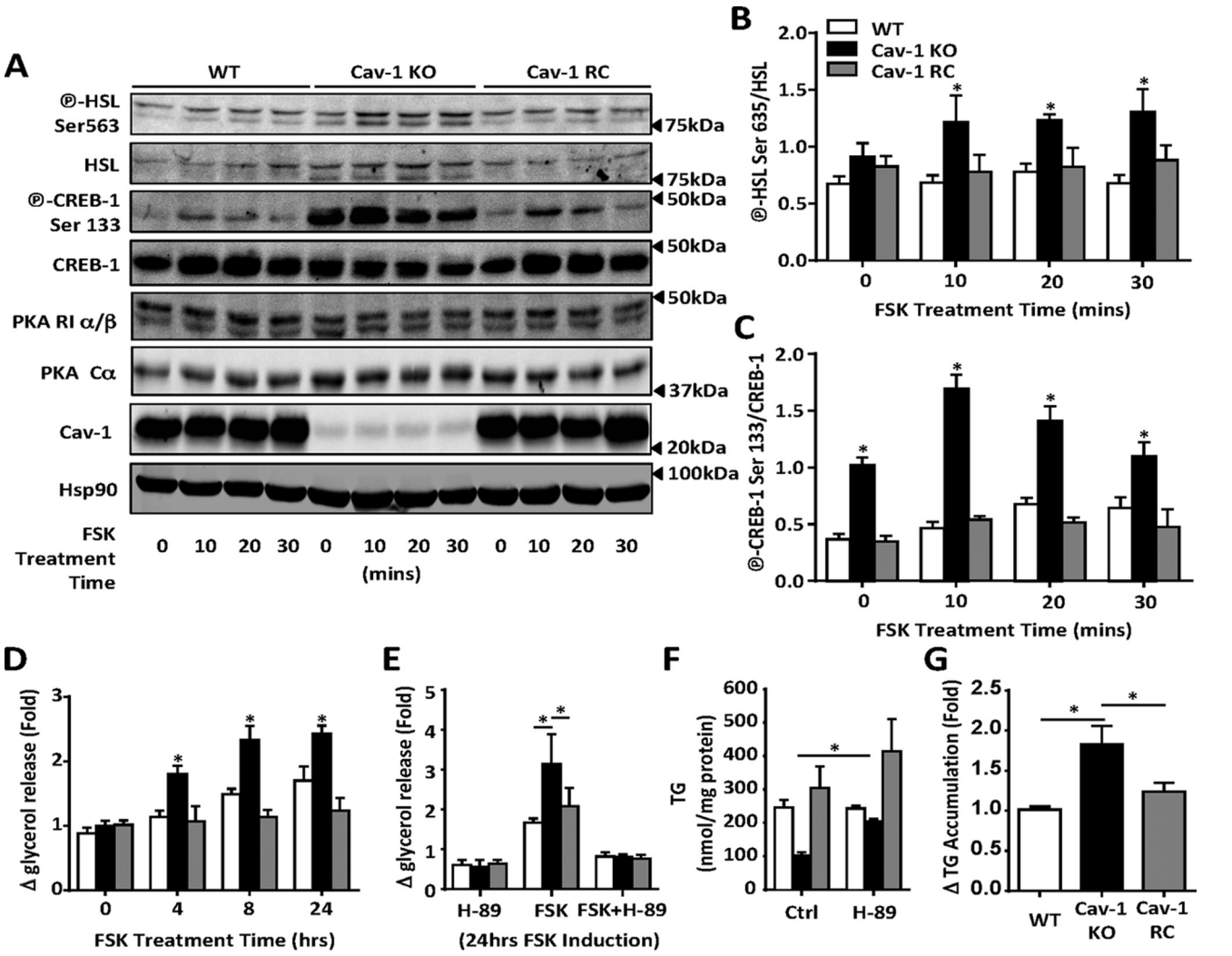

Figure 7. FSK-induced phosphorylation and lipolysis are enhanced in Cav-1 KO MLEC. *A*, EC were loaded with OA (1 mM overnight) and then stimulated with FSK (10 μM) to induce lipolysis via activation of PKA signaling. *B* and *C*, phosphorylation of CREB (*B*) and HSL (*C*) increased to a greater extent in Cav-1 KO EC after 10 min, as quantified. *D* and *E*, FSK-induced glycerol release was augmented in Cav-1 KO EC after 4 h, an effect abrogated by pretreatment with the PKA inhibitor H-89 (10 μM, *E*). *F*, H-89 inhibition of PKA enhanced TG accumulation after overnight OA treatment in EC lines. *G*, Cav-1 KO EC show a greater -fold increase in TG content. Western blot data are representative of three independent experiments. Data are expressed as mean ± S.E. (n = 3). Statistical analysis in *B–D* was determined by two-way ANOVA. *, $p < 0.05$ relative to WT and Cav-1 RC. Statistical analysis in *E–G* was determined by unpaired *t* test. *, $p < 0.05$.

bated at 4 °C for 20 min and centrifuged at 14,000 rpm for 10 min. Supernatants were collected, and protein concentration was measured with the DC™ protein assay kit (Bio-Rad.) Equal amounts of protein in each experiment were resolved by SDS-PAGE and transferred to nitrocellulose membranes for 2 h at 90 V using Mini Trans-Blot® Cell (Bio-Rad.) Membranes were blocked using 0.1% (w/v) casein (Bio-Rad) in TBS for 50 min and incubated with primary antibodies overnight at 4 °C. Membranes were washed with TBS-T (TBS solution containing 0.1% Tween 20) and incubated with conjugated secondary antibodies for 30 min at room temperature. Membranes were washed with TBS-T and developed using the Odyssey system (Li-Cor.) The densitometry of membranes was analyzed with ImageJ software (National Institutes of Health).

Lipid droplet formation and detection in vessels

Whole-mount thoracic aortas were isolated from 8- to 10-week-old WT, Cav-$1^{-/-}$, and Cav-1^{Rec} mice and incubated with OA conjugated to FA-free albumin (1 mM) in complete EBM-2 medium overnight in a 37 °C incubator with 5% CO_2, followed by *en face* immunostaining as described previously (16). Aortae were cut longitudinally, pinned down with EC facing upward, washed three times with PBS, and fixed with 4% paraformaldehyde in PBS. Fixed samples were further blocked with TNB blocking buffer (0.1 M Tris-HCl (pH 7.5), 0.15 M NaCl, and 0.5% (w/v) blocking reagent (PerkinElmer Life Sciences, FP1020)) overnight at 4 °C. Aortae were further incubated with anti-PECAM-1 antibody (EMD Millipore, MAB1398Z, 1:250) diluted in TNB blocking buffer overnight at 4 °C. Samples were washed three times with PBS and incubated with fluorescence-conjugated secondary antibody (Cy™3 AffiniPure Goat Anti-Armenian Hamster, Jackson ImmunoResearch Laboratories, 127-165-099, 1:200) at room temperature for 3 h. BODIPY 493/503 diluted in PBS at a final concentration of 4 μg/ml was applied for 30 min to delineate LD, and DAPI (Sigma, 0.1 ng/ml) was used to high-

Downloaded from http://www.jbc.org/ at Washington University on March 3, 2018

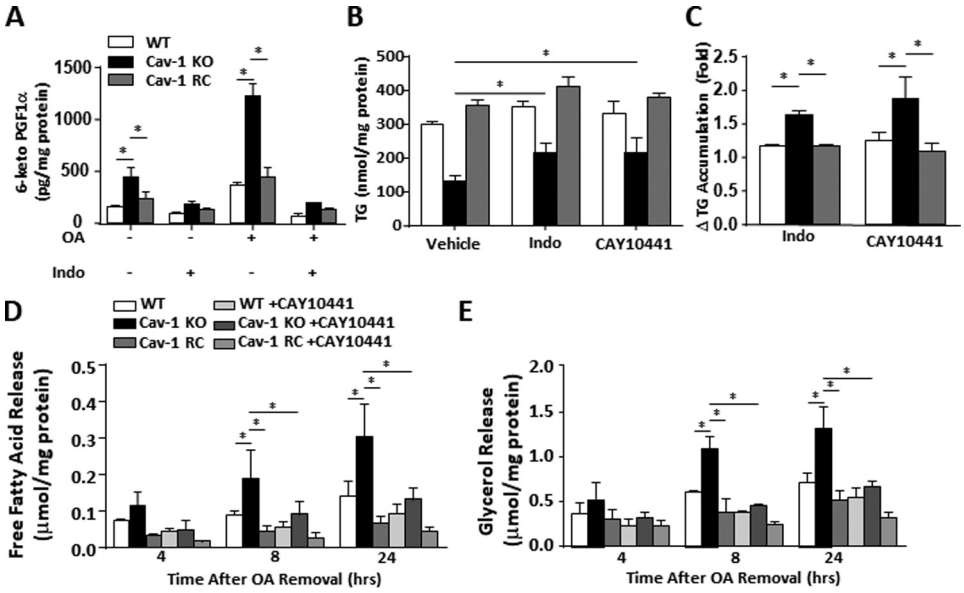

Figure 8. Loss of Cav-1 enhances basal and OA-stimulated levels of PGI_2 and regulates TG metabolism. *A*, the production of PGI_2, quantified by the stable breakdown product 6-keto PGF1α, is increased in Cav-1 KO EC. The production of PGI_2 is abolished by Indo (10 μM). *B*, blockade of either COX by Indo or the IP receptor antagonist CAY10441 (10 μM) increased TG content in three types of EC with a greater -fold induction (*C*) in Cav-1 KO EC. *D* and *E*, blockade of IP receptors by CAY10441 (10 μM) decreases free fatty acid and glycerol release in Cav-1 KO EC after 8 h. Data are expressed as mean ± S.E. ($n = 3–4$). Statistical analyses in *A–C* was determined by unpaired Student's *t* test and by two-way ANOVA in *D* and *E*. *, $p < 0.05$.

light the nucleus. Samples were mounted and imaged by confocal microscopy (Leica SP5).

Lipid droplet formation and detection in cultured EC

EC were grown to confluence on coverslips precoated with 0.1% gelatin in PBS solution. After the designated treatment, cells were washed with 3× PBS and fixed with 4% paraformaldehyde in PBS solution for 15 min. Fixed cells were washed with 3× PBS and stained with BODIPY 493/503 diluted in PBS at a final concentration of 0.1 μg/ml for 15 min to delineate LD and DAPI (Sigma, 0.1 ng/ml) to highlight the nucleus. Coverslips were mounted with Fluoromount^{TM} aqueous mounting medium (Sigma) and imaged by laser-scanning confocal microscopy (Leica SP5) in the sequential scan mode with an HCX PL APO λ blue 63×/1.40 oil objective lens at room temperature and analyzed with ImageJ software.

TG measurements

TG content was determined by mass spectrometry (Fig. 1*C*). TG content (Figs. 5*D*, 7*F*, and 8*B*) was determined by a colorimetric assay kit (BioVision Inc.) following the instructions of the manufacturer and normalized by total protein amount in each sample (determined by DC^{TM} protein assay kit (Bio-Rad).

Fatty acid uptake assay

The measurement of fatty acid uptake was performed as described previously with modifications (31). In brief, trace amounts of [^{14}C]oleic acid (PerkinElmer Life Sciences) mixed with non-radioactive oleic acid were dissolved in 10% free fatty acid BSA solution to a final concentration of 12 mM. This stock solution was further diluted with complete EBM-2 medium to a concentration of 1 mM and incubated with the confluent WT/Cav-1 KO/Cav-1 RC EC monolayer for 1, 2, 3, 4, and 24 h. The medium after incubation was collected, and aliquots were used to determine the remaining radioactivity. The uptake reaction was stopped by aspiration of the solution followed by addition of ice-cold solution containing 0.5% BSA and 200 μM phloretin for 2 min. Cells were washed three times with ice-cold PBS and lysed with 1 M NaOH. Protein concentration was determined using the DC^{TM} protein assay. Radioactivity in cell lysates and medium were determined with the addition of scintillation mixture solution (American Bioanalytical) using Tri-Carb 2900TR liquid scintillation analyzers. The percentage of fatty acid uptake was determined by radioactivity in cell lysates over total radioactivity added, normalizing to protein amount between each cell type.

DGAT activity assay

Enzymatic activity of DGAT was performed as described previously (32). 50 μg of protein lysate (in 250 mM sucrose and 50 mM Tris-HCl (pH 7.4) supplemented with complete protease inhibitors (Roche)) was incubated at 37 °C with 200 μM diacylglycerol (dissolved in acetone) and 25 μM [^{14}C]oleoyl-CoA. The reaction was stopped by methanol:chloroform (3:1), followed by addition of H_2O. The organic phase was extracted and dried by N_2. Dried lipids were suspended in chloroform and further subjected to TLC using hexane:diethylether:acetic acid (80:20:1) as solvent. The TLC plate was developed with a storage phosphor screen (Molecular Dynamics). Radioactivity was detected and imaged by Typhoon Trio Imager (GE Healthcare). The densitometry of TLC images was determined by Image Quant software (GE Healthcare).

Mass spectrometry

The TG content and molecular species distribution was determined using electrospray ionization–MS analysis as described previously with minor modifications (33–35). Briefly, lipids were extracted from EC using a modified Bligh and Dyer

Downloaded from http://www.jbc.org/ at Washington University on March 3, 2018

technique in the presence of the internal standard tri-17:1 TG. Because of the low abundance of TG species in non-OA-loaded cells, TG species were enriched into the hexane fractions through liquid/liquid partitioning using hexane–methanol–water (36). Electrospray ionization–MS analyses of hexane fractions (non-OA-loaded cells) or chloroform lipid extracts (OA-loaded cells) were performed utilizing a TSQ Quantum Ultra triple-quadrupole mass spectrometer (Thermo Fisher Scientific, San Jose, CA) equipped with an automated nanospray apparatus (Nanomate HD, Advion Bioscience Ltd., Ithaca, NY). TG molecular species were analyzed in the positive ion mode as Na^+ adducts or alternatively as Li^+ adducts (in the presence of a small amount of LiOH). TG molecular species identification and fatty acyl compositional analysis were performed in positive ion mode as Li^+ adducts or NH_4^+ adducts (in the presence of 10 mM ammonium acetate) using tandem mass spectrometry at collision energies of 35 or 25 electron volt, respectively.

Measurement of FFA and glycerol release

WT/Cav-1 KO/Cav-1 RC EC were grown to confluence and treated overnight with OA (1 mM). Medium containing OA was aspirated, washed with 2× PBS, and placed into serum-free EBM-2 medium containing 50 μM FFA–BSA. 1% of the medium was collected at the designated time points. FFA and glycerol concentration in the collected medium were determined using colorimetric assay kits (BioVision Inc.). FFA and glycerol release was normalized by total protein content in each sample, determined by DC™ protein assay kit (Bio-Rad).

Lipase activity assay

General lipase activity was measured based on the lipase activity colorimetric assay kit (Bio Vision Inc.) In brief, MLEC of the three genotypes were loaded with 1 mM OA overnight to induce lipolysis. Lysates were collected with the designated buffer, and protein concentration was determined by DC™ protein assay kit (Bio-Rad). 50 μg of total protein lysates was used in the reactions containing exogenous TG as substrates. Lipase activity was determined based on glycerol formation rate following the instructions of the manufacturer.

Cyclic AMP assay

EC were grown to confluence. After designated treatments, cells were lysed with 0.1 M HCl and chilled on ice. Lysates were collected, and cAMP was acetylated by addition of KOH and acetic anhydride. Protein concentration was determined by DC™ protein assay kit (Bio-Rad). Cyclic AMP was determined by cyclic AMP EIA kit (Cayman Chemical) and normalized by total protein content.

6-Keto PGF1-α assay

EC were grown to confluence, and the medium was replaced with medium or without 1 mM OA as well as with or without 10 μM indomethacin or 10 μM CAY10441. Conditioned medium was collected, and total protein amount was determined as described under "Western blot analysis". 6-keto PGF1-α concentration in the conditioned medium was determined by 6-keto PGF1-α EIA kit (Cayman Chemical) and normalized by total protein content.

Statistical analysis

Statistical analyses were performed using Prism 6 software (GraphPad) using tests as described in each figure. The data are presented as mean ± S.E.

Author contributions—A. K., M. Y. L., and W. C. S. conceptualization; A. K., M. Y. L., K. Y., and R. W. G. data curation; A. K., M. Y. L., K. Y., and R. W. G. formal analysis; A. K., R. W. G., and W. C. S. supervision; A. K., R. W. G., and W. C. S. funding acquisition; A. K., M. Y. L., R. W. G., and W. C. S. validation; A. K., M. Y. L., and K. Y. investigation; A. K., M. Y. L., K. Y., and R. W. G. methodology; A. K., M. Y. L., and W. C. S. writing-original draft; A. K. and W. C. S. project administration; A. K., M. Y. L., and W. C. S. writing-review and editing.

References

1. Palade, G. E. (1953) Fine structure of blood capillaries. *J. Appl. Phys.* **24,** 1424–1424
2. Parton, R. G., and Simons, K. (2007) The multiple faces of caveolae. *Nat. Rev. Mol. Cell Biol.* **8,** 185–194 CrossRef Medline
3. Drab, M., Verkade, P., Elger, M., Kasper, M., Lohn, M., Lauterbach, B., Menne, J., Lindschau, C., Mende, F., Luft, F. C., Schedl, A., Haller, H., and Kurzchalia, T. V. (2001) Loss of caveolae, vascular dysfunction, and pulmonary defects in caveolin-1 gene-disrupted mice. *Science* **293,** 2449–2452 CrossRef Medline
4. Razani, B., Engelman, J. A., Wang, X. B., Schubert, W., Zhang, X. L., Marks, C. B., Macaluso, F., Russell, R. G., Li, M., Pestell, R. G., Di Vizio, D., Hou, H., Jr., Kneitz, B., Lagaud, G., Christ, G. J., *et al.* (2001) Caveolin-1 null mice are viable but show evidence of hyperproliferative and vascular abnormalities. *J. Biol. Chem.* **276,** 38121–38138 Medline
5. Razani, B., Combs, T. P., Wang, X. B., Frank, P. G., Park, D. S., Russell, R. G., Li, M., Tang, B., Jelicks, L. A., Scherer, P. E., and Lisanti, M. P. (2002) Caveolin-1-deficient mice are lean, resistant to diet-induced obesity, and show hypertriglyceridemia with adipocyte abnormalities. *J. Biol. Chem.* **277,** 8635–8647 CrossRef Medline
6. Frank, P. G., Lee, H., Park, D. S., Tandon, N. N., Scherer, P. E., and Lisanti, M. P. (2004) Genetic ablation of caveolin-1 confers protection against atherosclerosis. *Arterioscler. Thromb. Vasc. Biol.* **24,** 98–105 CrossRef
7. Fernández-Hernando, C., Yu, J., Suárez, Y., Rahner, C., Dávalos, A., Lasunción, M. A., and Sessa, W. C. (2009) Genetic evidence supporting a critical role of endothelial caveolin-1 during the progression of atherosclerosis. *Cell Metab.* **10,** 48–54 CrossRef Medline
8. Farese, R. V., Jr., and Walther, T. C. (2009) Lipid droplets finally get a little R-E-S-P-E-C-T. *Cell* **139,** 855–860 CrossRef Medline
9. Wilfling, F., Wang, H., Haas, J. T., Krahmer, N., Gould, T. J., Uchida, A., Cheng, J. X., Graham, M., Christiano, R., Fröhlich, F., Liu, X., Buhman, K. K., Coleman, R. A., Bewersdorf, J., Farese, R. V., Jr., and Walther, T. C. (2013) Triacylglycerol synthesis enzymes mediate lipid droplet growth by relocalizing from the ER to lipid droplets. *Dev. Cell* **24,** 384–399 CrossRef Medline
10. Krahmer, N., Guo, Y., Wilfling, F., Hilger, M., Lingrell, S., Heger, K., Newman, H. W., Schmidt-Supprian, M., Vance, D. E., Mann, M., Farese, R. V., Jr., and Walther, T. C. (2011) Phosphatidylcholine synthesis for lipid droplet expansion is mediated by localized activation of CTP:phosphocholine cytidylyltransferase. *Cell Metab.* **14,** 504–515 CrossRef Medline
11. Ostermeyer, A. G., Paci, J. M., Zeng, Y., Lublin, D. M., Munro, S., and Brown, D. A. (2001) Accumulation of caveolin in the endoplasmic reticulum redirects the protein to lipid storage droplets. *J. Cell Biol.* **152,** 1071–1078 CrossRef Medline
12. Pol, A., Martin, S., Fernandez, M. A., Ferguson, C., Carozzi, A., Luetterforst, R., Enrich, C., and Parton, R. G. (2004) Dynamic and regulated asso-

Downloaded from http://www.jbc.org/ at Washington University on March 3, 2018

ASBMB

ciation of caveolin with lipid bodies: modulation of lipid body motility and function by a dominant negative mutant. *Mol. Biol. Cell* **15,** 99–110 Medline

13. Blouin, C. M., Le Lay, S., Lasnier, F., Dugail, I., and Hajduch, E. (2008) Regulated association of caveolins to lipid droplets during differentiation of 3T3-L1 adipocytes. *Biochem. Biophys. Res. Commun.* **376,** 331–335 CrossRef Medline
14. Cohen, A. W., Razani, B., Schubert, W., Williams, T. M., Wang, X. B., Iyengar, P., Brasaemle, D. L., Scherer, P. E., and Lisanti, M. P. (2004) Role of caveolin-1 in the modulation of lipolysis and lipid droplet formation. *Diabetes* **53,** 1261–1270 CrossRef Medline
15. Briand, N., Prado, C., Mabilleau, G., Lasnier, F., Le Lièpvre, X., Covington, J. D., Ravussin, E., Le Lay, S., and Dugail, I. (2014) Caveolin-1 expression and cavin stability regulate caveolae dynamics in adipocyte lipid store fluctuation. *Diabetes* **63,** 4032–4044 CrossRef Medline
16. Kuo, A., Lee, M. Y., and Sessa, W. C. (2017) Lipid droplet biogenesis and function in the endothelium. *Circ. Res.* **120,** 1289–1297 CrossRef Medline
17. Murata, T., Lin, M. I., Stan, R. V., Bauer, P. M., Yu, J., and Sessa, W. C. (2007) Genetic evidence supporting caveolae microdomain regulation of calcium entry in endothelial cells. *J. Biol. Chem.* **282,** 16631–16643 CrossRef Medline
18. Murata, T., Lin, M. I., Huang, Y., Yu, J., Bauer, P. M., Giordano, F. J., and Sessa, W. C. (2007) Reexpression of caveolin-1 in endothelium rescues the vascular, cardiac, and pulmonary defects in global caveolin-1 knockout mice. *J. Exp. Med.* **204,** 2373–2382 CrossRef Medline
19. Ring, A., Le Lay, S., Pohl, J., Verkade, P., and Stremmel, W. (2006) Caveolin-1 is required for fatty acid translocase (FAT/CD36) localization and function at the plasma membrane of mouse embryonic fibroblasts. *Biochim. Biophys. Acta* **1761,** 416–423 CrossRef Medline
20. Anthonsen, M. W., Rönnstrand, L., Wernstedt, C., Degerman, E., and Holm, C. (1998) Identification of novel phosphorylation sites in hormone-sensitive lipase that are phosphorylated in response to isoproterenol and govern activation properties *in vitro*. *J. Biol. Chem.* **273,** 215–221 CrossRef Medline
21. Shen, W. J., Patel, S., Natu, V., and Kraemer, F. B. (1998) Mutational analysis of structural features of rat hormone-sensitive lipase. *Biochemistry* **37,** 8973–8979 CrossRef Medline
22. Midgett, C., Stitham, J., Martin, K., and Hwa, J. (2011) Prostacyclin receptor regulation: from transcription to trafficking. *Curr. Mol. Med.* **11,** 517–528 CrossRef Medline
23. Parton, R. G., and del Pozo, M. A. (2013) Caveolae as plasma membrane sensors, protectors and organizers. *Nat. Rev. Mol. Cell Biol.* **14,** 98–112 CrossRef Medline
24. Pohl, J., Ring, A., Korkmaz, U., Ehehalt, R., and Stremmel, W. (2005) FAT/CD36-mediated long-chain fatty acid uptake in adipocytes requires plasma membrane rafts. *Mol. Biol. Cell* **16,** 24–31 Medline
25. Blouin, C. M., Le Lay, S., Eberl, A., Köfeler, H. C., Guerrera, I. C., Klein, C., Le Liepvre, X., Lasnier, F., Bourron, O., Gautier, J. F., Ferré, P., Hajduch, E., and Dugail, I. (2010) Lipid droplet analysis in caveolin-deficient adipocytes: alterations in surface phospholipid composition and maturation defects. *J. Lipid Res.* **51,** 945–956 CrossRef Medline
26. Martin, S., Fernandez-Rojo, M. A., Stanley, A. C., Bastiani, M., Okano, S., Nixon, S. J., Thomas, G., Stow, J. L., and Parton, R. G. (2012) Caveolin-1 deficiency leads to increased susceptibility to cell death and fibrosis in white adipose tissue: characterization of a lipodystrophic model. *PLoS ONE* **7,** e46242 CrossRef Medline
27. Deleted in proof
28. Chen, Y. W., Chen, Y. F., Chen, Y. T., Chiu, W. T., and Shen, M. R. (2016) The STIM1-Orai1 pathway of store-operated Ca^{2+} entry controls the checkpoint in cell cycle G_1/S transition. *Sci. Rep.* **6,** 22142 CrossRef Medline
29. Chen, S. F., Liou, J. Y., Huang, T. Y., Lin, Y. S., Yeh, A. L., Tam, K., Tsai, T. H., Wu, K. K., and Shyue, S. K. (2010) Caveolin-1 facilitates cyclooxygenase-2 protein degradation. *J. Cell. Biochem.* **109,** 356–362 Medline
30. Shiroto, T., Romero, N., Sugiyama, T., Sartoretto, J. L., Kalwa, H., Yan, Z., Shimokawa, H., and Michel, T. (2014) Caveolin-1 is a critical determinant of autophagy, metabolic switching, and oxidative stress in vascular endothelium. *PLoS ONE* **9,** e87871 CrossRef Medline
31. Stremmel, W., Strohmeyer, G., and Berk, P. D. (1986) Hepatocellular uptake of oleate is energy dependent, sodium linked, and inhibited by an antibody to a hepatocyte plasma membrane fatty acid binding protein. *Proc. Natl. Acad. Sci. U.S.A.* **83,** 3584–3588 CrossRef Medline
32. Yen, C. L., Monetti, M., Burri, B. J., and Farese, R. V., Jr. (2005) The triacylglycerol synthesis enzyme DGAT1 also catalyzes the synthesis of diacylglycerols, waxes, and retinyl esters. *J. Lipid Res.* **46,** 1502–1511 CrossRef Medline
33. Han, X., and Gross, R. W. (2001) Quantitative analysis and molecular species fingerprinting of triacylglyceride molecular species directly from lipid extracts of biological samples by electrospray ionization tandem mass spectrometry. *Anal. Biochem.* **295,** 88–100 CrossRef Medline
34. Han, X., Yang, K., and Gross, R. W. (2012) Multi-dimensional mass spectrometry-based shotgun lipidomics and novel strategies for lipidomic analyses. *Mass Spectrom. Rev.* **31,** 134–178 CrossRef Medline
35. Yang, K., Cheng, H., Gross, R. W., and Han, X. (2009) Automated lipid identification and quantification by multidimensional mass spectrometry-based shotgun lipidomics. *Anal. Chem.* **81,** 4356–4368 CrossRef Medline
36. Yang, K., Jenkins, C. M., Dilthey, B., and Gross, R. W. (2015) Multidimensional mass spectrometry-based shotgun lipidomics analysis of vinyl ether diglycerides. *Anal. Bioanal. Chem.* **407,** 5199–5210 CrossRef Medline

Downloaded from http://www.jbc.org/ at Washington University on March 3, 2018

Caveolin-1 regulates lipid droplet metabolism in endothelial cells via autocrine prostacyclin–stimulated, cAMP-mediated lipolysis

Andrew Kuo, Monica Y. Lee, Kui Yang, Richard W. Gross and William C. Sessa

J. Biol. Chem. 2018, 293:973-983.
doi: 10.1074/jbc.RA117.000980 originally published online December 4, 2017

Access the most updated version of this article at doi: 10.1074/jbc.RA117.000980

Alerts:
- When this article is cited
- When a correction for this article is posted

Click here to choose from all of JBC's e-mail alerts

This article cites 35 references, 16 of which can be accessed free at
http://www.jbc.org/content/293/3/973.full.html#ref-list-1

Downloaded from http://www.jbc.org/ at Washington University on March 3, 2018